MODELING SPACE-TIME DEPENDENT HELIUM BUBBLE EVOLUTION IN TUNGSTEN ARMOR UNDER IFE CONDITIONS

Qiyang Hu, Shahram Sharafat, Nasr M. Ghoniem

Mechanical and Aerospace Engineering Department, University of California, Los Angeles, CA 90095-1597, USA
huqy@ucla.edu

During Helium implantation or generation in finite geometries, space dependent parameters and features affect Helium transport through the material. Conventional kinetic rate-theory models assume strictly homogeneous field parameters and as such can not directly resolve space dependent phenomena of helium transport. The current work outlines a new approach to simulate space-dependent helium transport during irradiation in finite geometries. The model and the numerical code, called HEROS, are described and applied to simulate typical IFE relevant helium implantation conditions. A case study using the HAPL IFE reactor design is used to demonstrate the capabilities of the HEROS code. It is shown that the HEROS code is capable of simulating very complex transient and space dependent Helium transport in finite geometries, including the simultaneous transient production of defects and space- and time-dependent temperature and temperature gradients. Space dependent nucleation and growth of helium bubbles during implantation are modeled along with the impact of biased migration and coalescence of Helium bubbles.

I. INTRODUCTION

Helium production and helium bubble evolution in neutron-irradiated components has been the subject of intense research over the past decades. An example of severe impact on material performance by Helium implantation is in the First Wall of an Inertial Fusion Energy (IFE) reactor chamber. Following the implosion of the D-T pellet, X-rays, neutrons, high-energy Helium, and other charged particles arrive at the first wall within few microseconds (μs) with a frequency of 5 to 10 Hz. Implantation of low and high-energy (0.1 - 4 MeV) Helium ions can result in the formation of He bubbles a few μm beneath the surface. Long term operation causes the Helium bubbles to grow and can result in blistering of the surface, which can lead to surface exfoliation of about 1 to 2 μm thick layers in metals.[1] Blistering and exfoliation were observed in helium-implanted tungsten at doses of $10^{22}/m^2$ (Ref. 2, 3).

The evolution of microstructural features, such as bubble or blister formation in Helium implanted materials is a multiscale process in both space and time. Present day computational performance limitations do not allow simulation of microstructural evolution over engineering-relevant time scales (hours and beyond) starting with first principle calculations. Instead, an atomistic-to-continuum modeling method based on decoupled sequential simulation of energetics/kinetics, defect formation /clustering, and microstructural feature formation is employed. Pertinent information from the finer scale simulation is transferred to the next coarser but less computationally demanding scale. Of the aforementioned simulation methods, the Cluster Dynamics scale requires the smallest computational resources and can be used to investigate reactor lifetime scale phenomena and processes.[4,5,6]

In this work we present a modified Cluster Dynamics approach, which models space dependent microstructural changes based on kinetic rate theory. Thus, complex spatially dependent processes under fast and/or long term transient driving forces can now be simulated using minimal computational resources. A numerical code, called the HEROS code, which embodies the spatially dependent Cluster Dynamic theory has been developed and are briefly described in this work. A detailed description of the underlying HEROS code helium transport processes is given in Ref. 7. A case study is presented using IFE (Inertial Fusion Energy) Helium implantation in a tungsten armored chamber first wall. Spatially dependent- and transient implantation rates of Helium are followed by high temperatures and steep temperature gradients all within the span of a few μs and over the range a few micro-meters (μm) below the surface. Short annealing time of 0.1 to 0.2 sec occurs between successive shots. The HEROS code is used to simulate Helium bubble evolution and release through the free surface during these transient and spatially dependent conditions.

In Section IIA, a detailed description of the HEROS Helium transport model is given, followed by an outline of the numerical technique in Section IIB. In Section III,

results of applying the HEROS code to low energy (<100 keV) steady state helium implantation as well as high energy (<3 MeV) pulsed implantation in pure tungsten are compared with experimental data. Section IV shows conclusions.

II. HEROS HELIUM TRANSPORT MODEL

II.A. HEROS Master Equations

Ghoniem et al.[6] derived a set of hierarchical master equations (MEs), which successfully modeled the loss of helium to grain boundaries during irradiation. Later Sharafat et al.[5] augmented the MEs to include the effects of cascade induced interstitial- (CIIC) and vacancy clusters (CIVC). In the presence of helium these clusters were shown to have a significant effect on the bubble nucleation rate. In order to analyze space-dependent processes, these MEs were further modified by adding Drift and Diffusion terms for the most mobile species. First, we list here the set of MEs used in the HEROS code followed by an outline of the Drift and Diffusion terms.

The HEROS code uses a set of 13 master equations to model the evolution of the following 8 species: (1) unoccupied single vacancies; (2) single self-interstitial atoms; (3) interstitial helium atoms; (4) substitutional helium atoms; (5) di-interstitial helium atom clusters; (6) di-helium single vacancy clusters; (7) bubble nuclei (containing 3 helium atoms w/o a single vacancy); (8) large bubbles containing *m* helium atoms. Furthermore, five equations are used to analyze the (9) average matrix-bubble size; (10) average number of helium atoms in a matrix bubble; (11) amount of helium absorbed in grain boundaries; (12) average precipitate bubble radius; and (13) amount of helium in precipitate bubbles. In addition, the HEROS master equations analyze the sink-loss term associated with precipitate densities and grain boundaries. It is assumed, that on average each precipitate has one helium bubble attached to it. For a detail derivation of the spatially homogeneous rate equations the reader is referred to Ref. 6.

The following extended HEROS Cluster Dynamics equations include diffusion terms for vacancies, self-interstitial atoms (SIA), and interstitial helium atoms, as well as drift, diffusion, and coalescence terms for bubbles:

(1) Unoccupied vacancies (C_v):

$$\frac{dC_v}{dt} = (1-\varepsilon_v) f\dot{G} + (\beta e_1 + \delta) C_{gv} - \left(\alpha C_i + \beta C_g\right) C_v - \gamma C_v (C_s^v + C_{gv} + 2C_{2gv} + 2C_{2g} + 3C^* + C_i^l) + C_v^{eq} + D_v \frac{\partial^2 C_v}{\partial x^2} \quad (1)$$

(2) Self-interstitial atom (C_i):

$$\frac{dC_i}{dt} = (1-\varepsilon_i) f\dot{G} - \alpha C_i (C_v + C_{gv} + 2C_{2gv} + 3C^* + C_s^i + \sqrt{2} C_i^l) + C_i^{eq} + D_i \frac{\partial^2 C_i}{\partial x^2} \quad (2)$$

(3) Interstitial Helium atoms (C_g):

$$\frac{dC_g}{dt} = \dot{G}_{He} + (\beta e_1 + \delta + \alpha C_i) C_{gv} + (\beta e_2 + 2\delta) C_{2gv} + 3(\delta + \alpha C_i) C^* + 4\delta C_{2g} + 4\alpha C_i C_{2gv} + m\delta C_b + \delta M_{GB} + \delta M_{ppt} - \beta C_g \{\varepsilon C_b + C_v + 4\beta C_g + C_{gv} + 2C_{2g} + 2C_{2gv} + C_{GB} + \varepsilon_{ppt} C_{ppt} + 3C^*\} + D_g \frac{\partial^2 C_g}{\partial x^2} \quad (3)$$

(4) Substutional Helium atoms(C_{gv}):

$$\frac{dC_{gv}}{dt} = \beta C_g C_v + (\beta e_2 + 2\delta) C_{2gv} - C_{gv} \{\beta e_1 + \beta C_g + \delta + \alpha C_i\} \quad (4)$$

(5) A cluster of 2-Helium atoms and one vacancy (C_{2gv}):

$$\frac{dC_{2gv}}{dt} = \beta C_g C_{gv} + 3\delta C^* + 2\gamma C_v C_{2g} - C_{2gv} \left\{\beta e_2 + 2\delta + 2\beta C_g + 2\alpha C_i\right\} \quad (5)$$

(6) Di-interstitial Helium cluster (C_{2g}):

$$\frac{dC_{2g}}{dt} = 2\beta^2 C_g^2 + 3\alpha C_i C^* + 2\alpha C_i C_{2gv} - 2\left(\gamma C_v + \beta e_4 + \delta\right) C_{2g} \quad (6)$$

(7) Bubble nucleus concentration(C*):

$$\frac{dC^*}{dt} = 2\beta C_{2gv} C_g - 3C^* \left(\beta C_g + \gamma C_v + \alpha C_i + \delta\right) + 2\beta C_{2g} C_g \quad (7)$$

(8) Matrix bubble concentration (C_b):

$$\frac{dC_b}{dt} = \frac{12}{m}\beta C_g C^* + \frac{9}{m}\gamma C_v C^* - \frac{\partial}{\partial x}\left[\left(\frac{9 D_S a_o \Omega Q_S^*}{4\pi k T^2 R^4}\frac{dT}{dx} + \frac{3\Omega D_{vol} Q_V^*}{4\pi k T^2 R^3}\frac{dT}{dx}\right) C_b\right] - \left[4\pi(2R)(2D_b) + \pi(2R)^2\left(\frac{\partial}{\partial x}\left(\frac{9 D_S a_o \Omega Q_S^*}{4\pi k T^2 R^4}\frac{dT}{dx}\right)\right)\right] C_b^2 - \omega C_b C_{GB} \quad (8)$$

(9) Average number of Helium atoms in a matrix bubble (m):

$$\frac{dm}{dt} = \varepsilon_B \beta C_g - \delta m + C_b m\left[4\pi(2R)(2D_b) + \pi(2R)^2\left(\frac{\partial v}{\partial x}\Delta\right)\right] \quad (9)$$

(10) Average matrix bubble radius (R):

$$\frac{dR}{dt} = \frac{a^2}{48R}\left\{\gamma C_v - \alpha C_i - \gamma\left(e_3 - e_5\right)\right\} - \frac{R}{3C_b}\frac{dC_b}{dt} \quad (10)$$

(11) Helium in grain boundaries (M_{GB}):

$$\frac{dM_{GB}}{dt} = \beta C_{GB} C_g + m_1 \omega C_b C_{GB} - \delta M_{GB} \quad (11)$$

(12) Average precipitate bubble radius (R_{pptB}):

$$\frac{dR_{pptB}}{dt} = \frac{a^2}{\sqrt{\left(R_{pptB}^2 + r_p^2\right)}}\left\{\gamma C_v - \alpha C_i - \gamma\left(e_3' - e_4\right)\right\} \quad (12)$$

(13) Helium in precipitate bubbles (M_{ppt}):

$$\frac{dM_{ppt}}{dt} = \varepsilon_{pptB}\beta C_{ppt} C_g - \delta M_{ppt} \quad (13)$$

For detailed descriptions of the equations and terms the readers should refer to Ref. 7. Equations (1), (2), (3), and (8) represent the mobile species of vacancies, self-interstitials, interstitial helium atoms, and matrix bubbles, respectively. The difference between present equations describing C_v, C_i, C_g, and rate-theory based models is that we included here the space-dependent diffusion term due to the flux ($\nabla \cdot J$) of these mobile species. The bubble concentration rate equation (Eq. (8)) is augmented with drift, diffusion, and a coalescence terms.

The reaction rate equations (1) through (7) represent the bubble nucleation process, while equations (8) through (10) represent average bubble concentrations, average sizes, and helium content. The detailed discussion about the choice and validity of parameter and constants can be referred to Ref. 7.

Di-helium clusters, Eq. (6) are included in the rate equations, although the low binding energies for di-helium clusters make them unstable at high temperatures.[8] However, at low temperatures the di-helium cluster will play a role in nucleating bubbles because single helium atoms or di-helium clusters force or stabilize cavity nucleation. A single vacancy plus di-helium cluster ($C_{v,2g}$) has a strong backward reaction rate and as such can not be considered as a stable helium bubble nucleus. Therefore, we define a stable helium bubble nucleus (C*) as one containing at least 3 helium atoms and more than one vacancy, as represented by Eq. (7).

II.B. HEROS Numerical Scheme

The Master Equations (Eqs. (1)-(13)) represent the microstructure and Helium-bubble evolution during irradiation. If these equations are solved independent of space, using homogeneous field parameters and ignoring the spatial fluxes of migrating species, the model will describe a spatially homogeneous microstructure evolution. This approach could not be used to simulate driven- or biased bubble migration processes. However, by discretizing space this set of Master Equations can be solved to simulate both, spatial- and time dependent processes.

The HEROS codes discretizes space into predefined spatial bins and then solves the ME's within each bin, while keeping track of all mobile species fluxes across bin boundaries (vacancies, SIAs, interstitial Helium, and matrix bubbles). Although within each spatial bin the ME's are solved using homogeneous field parameters, the net flux of migrating species across the bins imparts a space-dependent simulation of the microstructure evolution as a function of space and time. Provided the spatial bin sizes are chosen fine enough, such that the details and the extend of external driving forces are captured, the solution will model space dependent processes.

By discretizing space, the flux of mobile species crossing bin boundaries are modeled with respective diffusion and drift components. Thus, the Master Equations simulate the transport of mobile species through space, although the MEs are solved using homogeneous field parameters within each bin. Solved in this manner, the impact of driving forces, such as temperature and stress gradients across a finite geometry or the spatial variations in production rates, such as in near surfaces can be analyzed. Furthermore, local variations in microstructural features (sinks, grain boundaries, precipitates, etc.) can also be included to reflect the impact of space-dependent material variations. Diffusion coefficients of the primary mobile species (vacancies, self-interstitial atoms, interstitial helium atoms) are modeled using experimentally measured activation energies. Bubble migration processes based on brownian motion, surface diffusion, and volume diffusion are formulated and solved independently in each bin. Bubble migration due to Vapor Transport has been neglected; however it can readily be incorporated into the Master Equation.[9]

III. MODELING IFE HELIUM IMPLANTATION

The High Average Power Laser (HAPL) program is a multi-institutional effort to develop Laser Inertial Fusion Energy.[10] The implosion of the D-T target produces a spectrum of neutrons, X-rays, and charged particles, which arrive at the first wall of a 5 to 10 m radius chamber at different times within about 2.5 μs at a frequency of 5 to 10 Hz. Helium is one of several high-energy charged particles impinging on the candidate tungsten armored low activation ferritic steel FW. The energy spread of the fast burn and slow burn (debris) helium (^{4}He) energies as shown in Ref. 0, which results in a rapid space-time dependent implantation profile to a depth of about 10 μm below the tungsten surface. Consequently, the rate of helium implantation varies significantly throughout the implanted region. Helium implantation times last about 0.1 μs, which are followed by an annealing time of about 0.1 to 0.2 s between shots.

Fig. 1 shows results of a FEM analysis of the spatial temperature profiles near the surface of the Tungsten armor (154 MJ D-T target; 6.5 m radius chamber).[12] We keep the temperature on boundaries fixed at 400°C. Fig. 1 will provide an input to the above MEs.

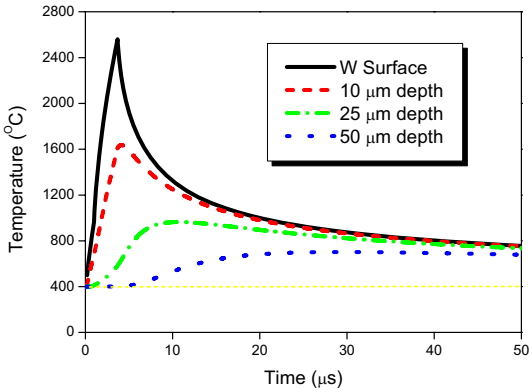

Fig. 1 Space- and time-dependent temperature profiles in the surface of a tungsten armor of a 10 m radius chamber exposed to a 154 MJ target.[0]

The implanted helium ion energies range from a few keV to several MeV. Helium implantation depths were estimated using the SRIM-2003 Monte Carlo computer program.[13] The total space-dependent implantation profile from all ^{4}He (all energies) is shown in Fig. 2.

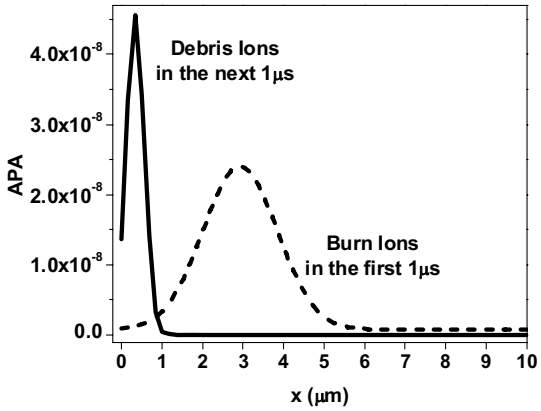

Fig. 2 Total per shot ^{4}He implantation profile in a tungsten coated FW of a 6.5 m radius chamber from a 154 MJ D-T target.

TABLE I. Damage parameters

Parameter	Value	Units
Helium atoms per shot	1.96×1020	Ions
FW solid surface area	531	m^2
Helium penetration depth	5×10^{-6}	m
Total W-Volume containing helium	2655	cm^3
Helium concentration in W per shot	7.38×10^{16}	cm^{-3}
Fractional He concentration per shot	1.17	appm
Vacancies produced per He ion	308	vacancy
H produced per He ion	60	atoms
Displacement damage per shot	4.30×10^{-4}	dpa
Pulse on-time	1.90×10^{-6}	s
Instantaneous damage rate	226	dpa/s
Helium rate	2725	appm/dpa
Ave. helium implantation rate (5 Hz)	5.85	appm/s
Ave. damage (5Hz)	2.15×10^{-3}	dpa/s

The implantation of high energy Helium results in significant self-damage inside the host material. Implantation parameters due to a 154 MJ D-T target in tungsten are given in Table I.

A typical HEROS code simulated bubble evolution is depicted in Fig. 3. The time sequence of the space-dependent evolution of helium bubble concentration is shown as a function of depth from the implanted tungsten surface. Within ~10^{-8} sec of the high energy (> 1 MeV) helium implantation a distinct bubble concentration peak occurs at ~3 μm from the surface. This peak in bubble concentration coincides with the location of the peak of implanted helium atoms (Fig. 2).

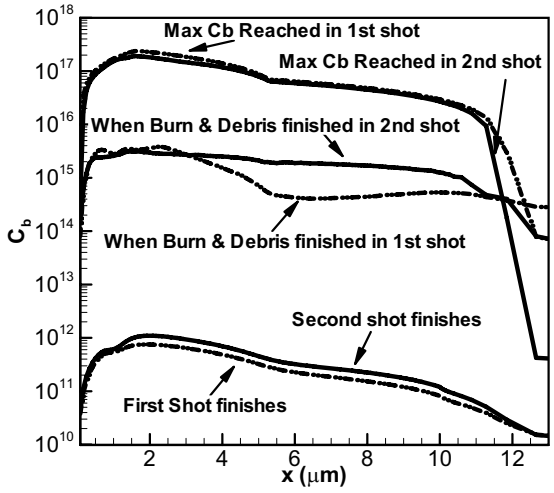

Fig. 3 Result of HEROS code simulation: time sequence of space-dependent Helium bubble concentration evolution in Tungsten caused by the transient implantation of helium from a 154 MJ D-T target in a 6.5 m radius chamber.

At ~0.7×10^{-6} sec following helium implantation, the number density of the helium bubbles has reached a peak of about 10^{17} per cm^3. Although maximum Helium implantation depth is ~5 μm, at 0.7 x 10^{-6} s helium bubbles are present to a depth of about 10 m (bubble density C_b ~ 10^{16} cm^{-3}). During the initial stages of bubble evolution atomic defects dominate HeV cluster formation. Ghoniem et al.[14], have shown that at elevated temperatures and in the presence of excess vacancies Helium diffuses via a vacancy mechanism coupled with a dissociative mechanism. Table I lists the number of vacancies produced per high energy Helium ion (1 to 3 MeV) to be of the order of 300 (vacancy supersaturation). Thus, effective migration of Helium during the initial stages of implantation is expected to be of the order of the self-diffusion rates. This explains the rapid buildup of bubble concentrations at a distance twice the implantation depth (Fig. 3; t = 0.4×10^{-6} s).

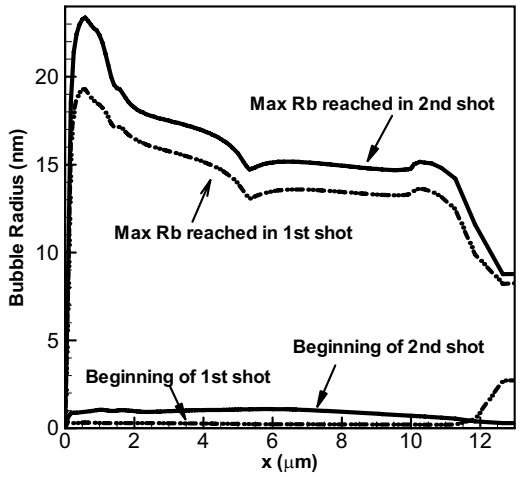

Fig. 4 HEROS code simulation results showing the time sequence of average Helium bubble radius evolution as a function of implantation depth.

It is interesting to note, that during debris ion implantation the concentration of existing bubbles decreases rapidly and after ~1 ms the peak bubble concentration has dropped from a high of $\sim 10^{17}$ cm^{-3} to about 3×10^{15} cm^{-3}. At the end of Helium implantation, annealing starts and by 0.8 ms the bubble concentration has been reduced to very low levels of $\sim 10^{13}$ cm^{-3} a 4 orders of magnitude drop from the peak. The average bubble radii are also calculated and the time sequence is shown in Fig. 4.

IV. CONCLUSIONS

Modeling space dependent Helium bubble evolution is critical for understanding the transport of Helium in near surface implantation experiments. Furthermore, the spatially dependent Helium bubble migration due to external driving forces, such as temperature- or stress gradients can only be modeled using space dependent models. This work outlines a new approach, which uses a simplified system of Master Equations in conjunction with a spatial finite difference scheme to model space dependent Helium transport during irradiation. The new method culminated in the development of the HEROS code, which was applied to model the transient and rapid Helium implantation conditions of a FW chamber of an typical IFE reactor.

It was shown that the HEROS code provides a framework for simulating very complex transient spatial Helium implantation profiles, including the simultaneously transient production of defects and space dependent temperature and temperature gradients. Thus, both space dependent and driven migration and coalescence of Helium bubbles can now be modeled using a simple set of Master Equations after calibrating the parameters from experimental results.

ACKNOWLEDGMENTS

The authors wish to express their gratitude to Dr. B. Singh and Dr. S. Gobolov for the many valuable discussions, comments, and suggestions made during the course of this work. Research was supported by the US Naval Research Laboratory. Grant DE-FG03-98ER54500 with UCLA.

REFERENCES

1. M. KAMINSKY and S.K. DAS, *J. Nucl. Mat.* **76-77** 256 (1978).
2. K. TOKUNAGA, O. YOSHIKAWA, K. MAKISE and N. YOSHIDA, *J. Nucl. Mat.* **307**, 130 (2002).
3. G.M. MCCRACKEN, *Rep. Prog. Phys.* **38** 241 (1975).
4. A.V. BARASHEV, S.I. GOLUBOV, D.J. BACON, P.E.J. FLEWITT and T. A. LEWIS, *Acta Mat.*, **52**, 4 877 (2004).
5. S. SHARAFAT and N.M. GHONIEM, *J. Nucl. Mater.*, **283** 789 (2000).
6. N.M. GHONIEM, J.N. ALHAJJI, and D. KALLETA, *J. Nucl. Mater.* **136**, 192-206 (1985).
7. S. SHARAFAT, Q. HU, and N. GHONIEM, "HEROS: A Spatial- and Temporal Helium Bubble Evolution and Resolution Code," *J. Nucl. Mat.* (2007), submitted.
8. H. TRINKAUS, *J. Nucl. Mat.*, **118**, 39 (1983).
9. F.A. NICHOLS, *J. Nucl. Mat.* **30**, 143 (1969).
10. J.D. SETHIAN M. FRIEDMAN, R.H. LEHMBERG, M. MYERS, S.P. OBENSCHAIN, J. GIULIANI, P. KEPPLE, A.J. SCHMITT, D. COLOMBANT, J. GARDNER, F. HEGELER, M. WOLFORD, S.B. SWANEKAMP, D. WEIDENHEIMER, D. WELCH, D. ROSE, S. PAYNE, C. BIBEAU, A. BARAYMIAN, R. BEACH, K. SCHAFFERS, B. FREITAS, K. SKULINA, W. MEIER, J. LATKOWSKI, L.J. PERKINS, D. GOODIN, R. PETZOLDT, E. STEPHENS, F. NAJMABADI, M. TILLACK, R. RAFFRAY, Z. DRAGOJLOVIC, D. HAYNES, R. PETERSON, G. KULCINSKI, J. HOFFER, D. GELLER, D. SCHROEN, J. STREIT, C. OLSON, T. TANAKA, T. RENK, G. ROCHAU, L. SNEAD, N. GHONEIM and G. LUCAS, *Nucl. Fusion* **43**, 1693 (2003).
11. Threat spectra posted at http://aries.ucsd.edu/ARIES /WDOCS/ARIES-IFE/SPECTRA/
12. S. SHARAFAT, N. M. GHONIEM, MICHAEL ANDERSON, BRIAN WILLIAMS, JAKE BLANCHARD and LANCE SNEAD, *J. Nucl. Mat.* **347** 217 (2005)
13. J.F. ZIEGLER, SRIM-2003, "The Stopping and Range of Ions in Matter," Available from: http://www.srim.org/, 2003.
14. N.M. GHONIEM, S. SHARAFAT, J.M. WILLIAMS and L.K. MANSUR, *J. Nucl. Mater.* **117**, 96 (1983).